Impact of increased atmospheric moisture on the precipitation depth caused by Hurricane Ivan (2004) over a target area

Mathieu Mure-Ravaud *, M. Levent Kavvas, Alain Dib

University of California, Davis, 1 Shields Ave, Davis, CA 95616, United States of America

HIGHLIGHTS

- Atmospheric moisture was increased in the simulation of Hurricane Ivan (2004)
- A target area was selected and rainfall depth over this target was maximized
- This maximization was done using a physically based storm transposition method
- The largest rainfall depth was obtained for no moisture increase
- Moisture just one aspect explaining rain intensity; Storm track is more important.

GRAPHICAL ABSTRACT
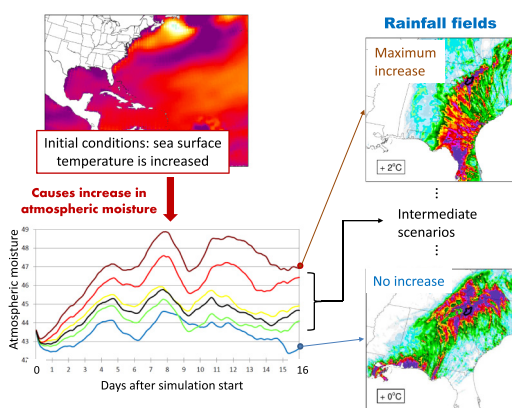
ABSTRACT

In this article, numerical experiments are performed to investigate the effects of increasing atmospheric moisture on the precipitation depth (PD) produced by Hurricane Ivan (2004) over a target area, chosen as the drainage basin of the city of Asheville, NC. Atmospheric moisture was increased indirectly by increasing the sea surface temperature (SST) in the simulation initial conditions, and by letting the regional atmospheric model adjust the atmospheric fields to the SST perturbation. The SST was increased in two ways: 1) using spatially constant increments and 2) using a climate change perturbation field obtained from a climate projection. For each SST scenario, the PD over the target area was maximized by using a physically based storm transposition method. Although the mean PD, that was obtained by averaging over all shifting increments, increased with SST, the maximum PD was obtained for the case of no SST increase. It was found that, in the case of no SST increase, the worst-case tropical cyclone track was significantly different than in the SST increase scenarios. In particular, in this case, the storm spent a longer time in the simulation inner domain, thus spawning a larger PD over the target area.

© 2019 Elsevier B.V. All rights reserved.

1. Introduction

Hurricane Ivan (2004) was a classical, long-lived Cape Verde[1] hurricane that reached Category 5 strength on the Saffir-Simpson Hurricane Wind Scale three times. It was the strongest hurricane on record that far south east of the Lesser Antilles and caused considerable damage and loss of life as it passed through the Caribbean Sea. Ivan made landfall in the U.S. as a Category 3 hurricane just west of Gulf Shores, AL on September 16th and caused extensive damage to coastal and inland areas, including the destruction of millions of acres of woodlands and forests. It spawned 117 tornadoes, severe storm surge, intense precipitation[2] (IP), and extensive freshwater flooding (Stewart, 2004).

Given the destructive impact of Hurricane Ivan, it is interesting to understand how the storm would have behaved in a moister environment. Would the damage and precipitation from the storm have been more severe under increased moisture conditions? Such an intensification of the precipitation depth (PD) field can be legitimately expected because moisture convergence generally plays a key role in the generation of IP in tropical cyclones (TCs) (Mure-Ravaud et al., 2019b). In particular, Mure-Ravaud (2019) showed that there was a strong correlation between the PD and the divergence of the vertically integrated vapor transport[3] (IVT) in Hurricane Ivan. More specifically, the regions of IP overall closely matched the regions of largest IVT convergence (i.e. the additive inverse of the IVT divergence). These results are reported in Appendix A.

Thus, this article investigates whether increased atmospheric moisture conditions actually translate into an intensification of Hurricane Ivan's PD field by means of a regional atmospheric model's (RAM) simulations. This study may be of interest for several applications. First, in the context of a changing climate, and more specifically of global warming, the capacity of the atmosphere to hold water is expected to increase in the future, which would in turn result in an increase of the IVT in TCs, and ultimately in an increase of the PD from these storms through IVT convergence. As such, the present study can be seen as an investigation into what to expect in terms of IP if Hurricane Ivan occurs again in the future.

This study is also of interest with regards to estimating Probable Maximum Precipitation[4] (PMP) in regions receiving their most IP from TCs and their remnants. In fact, there are several methods for PMP estimation which are detailed, for example, in the *Manual on Estimation of Probable Maximum Precipitation* by the World Meteorological Organization (2009). Such methods have been used for several decades to provide PMP estimates in several countries such as the U.S. (Corrigan, 1999; Hershfield, 1965, 1961), China (Zhan and Zhou, 1984), India (Kulkarni et al., 2010; Rakhecha and Soman, 1994), Thailand (Tingsanchali and Tanmanee, 2012), and Spain (Casas et al., 2008, 2011).

A common method which has been widely used to provide PMP estimates for sub-basins of the Tennessee River Watershed, where our target area (see Section 2) is located, is the generalized method (or generalized estimation). The main steps for PMP estimation via this method include (World Meteorological Organization, 2009):

1. Determination of high-efficiency storms (i.e. storms for which precipitation efficiency has reached its maximum);
2. Moisture maximization;
3. Transposition of the PD field of moisture-maximized, high-efficiency storms in meteorologically homogeneous zones;
4. Enveloping, where PD is maximized for various areas and durations using depth-area-duration (DAD) curves;
5. Estimating the PMP by retaining the most IP that comes from the above DAD enveloping values for the design watershed.

A certain number of assumptions and simplifications are made at each step of the above process, which may not be legitimate for the case of TCs. For example, Mure-Ravaud et al. (2019a) proposed a physically based alternative to the traditional storm transposition (ST) approach for maximizing the PD from a TC over a target area. This method is based on the shifting of the TC vortex in the simulation initial conditions (ICs). More precisely, the TC at the simulation start date is separated from its background environment, then shifted, and finally recombined with the background environment, after which the RAM is run as usual to simulate the TC and its PD field. This method takes advantage of the strong nonlinearity involved in the dynamics and thermodynamics of TCs: a small change in the location of the TC vortex in the ICs may bring about significant changes in the TC track, thus allowing the storm to move over the target area. This method is illustrated in Fig. 1.

Mure-Ravaud et al. (2019a) showed that the PD field of a TC can change dramatically in terms of its structure and intensity after its physically based ST (PB-ST). This is because the spatiotemporal behavior of the IVT field and its divergence may vary significantly as the TC interacts with its new environment, including the local topography and other synoptic and mesoscale systems. A corollary is that a TC which did not initially produce IP might, in fact, have produced IP if it had had a different track. These findings put into question the first step of the generalized method because storms which did not reach maximum precipitation efficiency may still produce a very large PD over the target area after PB-ST. On the other hand, because of the aforementioned large sensitivity of a TC track to many factors, such as the location of the initial TC vortex, a TC which affected a region far from the target area may still be brought to the target area after PB-ST. This also puts into question the legitimacy of restricting the ST limits to *meteorologically homogeneous zones* (see Step 3 of the generalized method) in the case of the ST of TCs.

As far as it is concerned, the moisture maximization step (Step 2) is a linearized meteorological approach that maximizes IP from a storm by the ratio of the maximum to the actual precipitable water[5] (PW). As measurements or estimates of PW are usually unavailable due to the absence or sparsity of upper-air observational networks, maximum values of atmospheric water vapor used for storm maximization are generally

---

[1] A Cape Verde-type hurricane is an Atlantic basin tropical cyclone (TC) that develops into a tropical storm fairly close (<1000 km) to the Cape Verde Islands and becomes a hurricane before reaching the Caribbean (definition from the Hurricane Research Division website).

[2] Strictly speaking, *precipitation* refers to any type of water that forms in the Earth's atmosphere and then drops onto the surface of the Earth, the most common types of precipitation being rain, hail, and snow (definition from the National Geographic Society). However, rain is generally the prevailing type of precipitation produced by tropical cyclones in the United States. As a result, in this article, *precipitation* will refer to rain only.

[3] The IVT field (or moisture advection field) is a two-dimensional vector field which quantifies the horizontal transport of water vapor by the wind. The IVT is given by the following relationship:

$$\mathrm{IVT} = \int_{z=0}^{z_{top}} \rho_v\, \mathbf{U}\, \mathrm{d}z = \int_{z=0}^{z_{top}} q_v\, \rho\, \mathbf{U}\, \mathrm{d}z = \frac{1}{g} \int_{p=0}^{p_{surf}} q_v\, \mathbf{U}\, \mathrm{d}p$$

where z is the vertical coordinate (height), z_{top} is the height of the top of the atmosphere, ρ_v is the density of the water vapor, q_v is the specific humidity, ρ is the density of air, p is pressure, p_{surf} is the surface pressure, g is the gravitational acceleration, and $\mathbf{U}$ is the wind velocity vector. Note that the hydrostatic equilibrium assumption was used to go from the second expression to the last expression, where the integral is expressed in pressure coordinates. This change of coordinates in the integral was performed because it is easier to calculate the IVT using this form.

[4] Probable Maximum Precipitation (PMP) is the PD for a given duration meteorologically possible for a design watershed or a given storm area at a particular location at a particular time of year, with no allowance made for long-term climatic trends (World Meteorological Organization, 2009).

[5] PW is the atmospheric water vapor contained in a vertical column of unit cross-sectional area extending between any two specified levels, commonly expressed in terms of the height to which that water substance would stand if completely condensed and collected in a vessel of the same unit cross section. Besides, the total PW is that contained in a column of unit cross section extending all of the way from the earth's surface to the *top* of the atmosphere (definition from the Meteorology Glossary of the American Meteorological Society). Total PW is often simply referred to as *PW*.
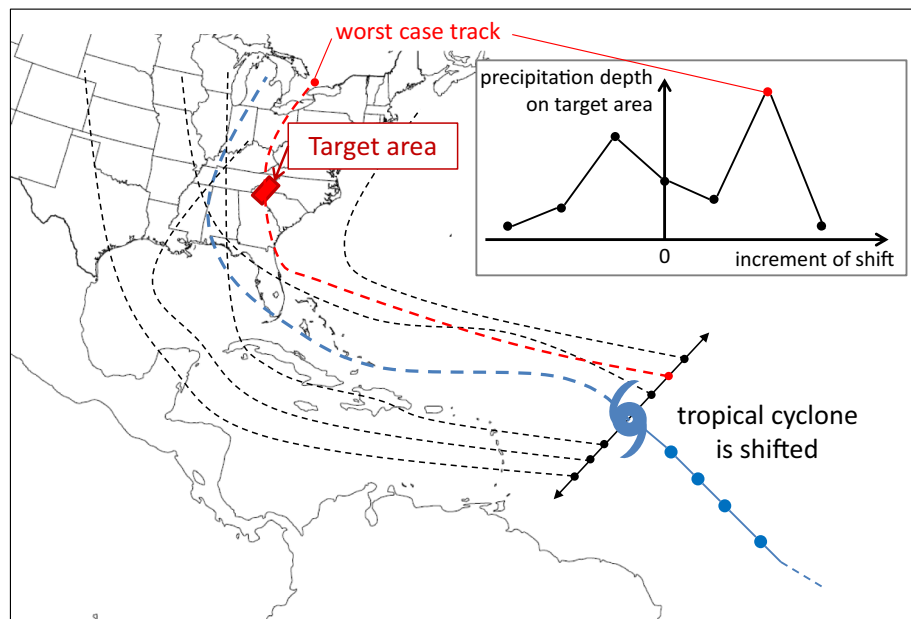
Fig. 1. Illustration of the physically based storm transposition (PB-ST) method of Mure-Ravaud et al. (2019a): the PD from a TC over a target area (red region) is maximized by modifying the system's track. This is done by shifting the TC vortex in the simulation initial conditions (ICs) in a direction orthogonal to the TC track.

estimated from maximum persisting 12-h 1000-hPa dewpoints[6] obtained from surveys of long records (50 or more years) at several stations in the problem area, based on the assumption of a saturated pseudo-adiabatic atmosphere (World Meteorological Organization, 2009). Thus, this article also helps to assess the legitimacy of the conventional moisture maximization: does an increase in the moisture inflow into a given storm necessarily translate into an increase in precipitation?

Section 2 of this article presents the modeling framework. Section 3 discusses the method used to increase atmospheric moisture. Section 4 provides the simulation results. Section 5 discusses these results. Finally, Section 6 offers the conclusions.

2. Modeling framework

The modeling framework used for the simulation of Hurricane Ivan is the same as in Mure-Ravaud et al. (2019a). In particular, the RAM used for this study is the Weather Research and Forecasting (WRF) model (Skamarock and Klemp, 2008) version 3.7. The WRF model is a numerical weather prediction model used for operational and research applications to enhance the prediction and understanding of mesoscale (i.e. regional scale) weather and to accelerate the transfer of research advances into operations. The WRF model is a fully compressible and nonhydrostatic model. It is conservative for scalar variables and uses a terrain-following mass-based vertical coordinate system.

Initial and boundary conditions for the WRF model simulations were obtained from the National Centers for Environmental Prediction (NCEP) Climate Forecast System Reanalysis (CFSR; Saha et al., 2010a, 2010b, 2011, 2014). CFSR is provided at $0.5° \times 0.5°$ (approximately

56 km $\times$ 56 km) horizontal resolution, uses 37 atmospheric pressure levels, and a 6-h temporal resolution.

Three nested domains were used for the dynamical downscaling of CFSR with WRF (Fig. 2), and the model was run with two-way nesting.[7] The outermost domain had a horizontal resolution of 45 km, the intermediate domain had a resolution of 15 km, and the inner domain had a resolution of 5 km. In addition, 38 atmospheric model levels were used in the vertical with a pressure top of 50 mbar, along with a time step of 3 min.

Table 1 provides the WRF model options (parameterization schemes) used for the simulation of Hurricane Ivan. A justification for the choice of these schemes is given in Appendix A. The simulation start date was taken as 09/06/2004 00:00 UTC, which is about 10 days before the time of landfall. At that time, Hurricane Ivan was located in the tropics, off the coasts of French Guiana and Suriname.

The target area selected in this study for the PB-ST was the drainage basin of the city of Asheville, NC (Fig. 3). This watershed has a surface area of approximately 2400 km^2 (930 mi^2) and contains 88 nodes of the simulation inner domain.

For each of the sea surface temperature (SST) increase scenarios discussed in the next section, Hurricane Ivan was shifted in a direction orthogonal to its direction of propagation (similar to Fig. 1) at the simulation start date by first using 35 increments of shift (including zero shift) from 2.02°W/8.72°S to 2.02°E/8.72°N. The WRF model was run for each of these increments of shift and the maximum 72-h PD over the target area was calculated for every simulation, which corresponds to the 72-h time window containing the largest basin average (BA) PD. Refinement steps were then performed around the local maxima of the graph of the 72-h BA PD as a function of the shifting amount (see for example the graph in the top right corner of Fig. 1 as an illustration) in order to further maximize the BA PD. Such a refinement was done by considering the increments of shift halfway between the local maxima and the neighboring increments of shift. It is noted that the

---

[6] The dewpoint is the temperature the air needs to be cooled to (at constant pressure) in order to achieve a relative humidity (RH) of 100%. At this point the air cannot hold any more water in the gas form. If the air were to be cooled even more, water vapor would have to come out of the atmosphere in the liquid form, usually as fog or precipitation. The higher the dewpoint rises, the greater the amount of moisture in the air (definition from the National Weather Service).

[7] *Two-way nesting* means that the nested domains were run simultaneously and communicated with each other, which differs from a *one-way nesting* modeling framework for which the nested domains are run separately and sequentially starting with the outer domain.
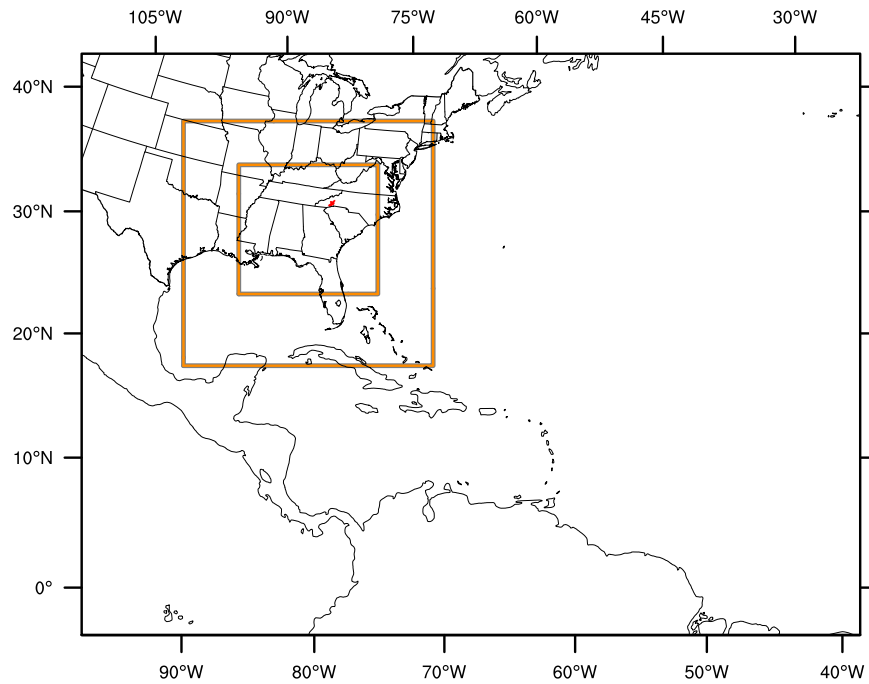
Fig. 2. Nested domains used for the simulation of Hurricane Ivan. The outer domain (45 km resolution) is composed of 160 × 120 nodes, the intermediate domain (15 km resolution) of 154 × 151 nodes, and the inner domain (5 km resolution) of 256 × 238 nodes. The small red area in western North Carolina is the target watershed, presented in Fig. 3.

results for the PB-ST of Hurricane Ivan in the case of no SST increase are already presented in Mure-Ravaud et al. (2019a).[8]

3. Increasing atmospheric moisture

Atmospheric moisture in the simulation domains was increased indirectly by increasing the SST in the simulation ICs, and by letting the WRF model adjust the atmospheric fields to the SST perturbation. The SST at the simulation start date (shown in Fig. 4a) was increased in two ways. First, it was increased by spatially constant increments: 0.5 °C, 1 °C, 1.5 °C, and 2 °C. Secondly, a climate change (CC) SST perturbation field (Fig. 4b) was added to it. This spatially varying CC perturbation field was obtained by subtracting the mean SST field in the Community Climate System Model version 4[9] (CCSM4) using Representative Concentration Pathway[10] (RCP) 4.5 during 2005–2024 from the mean SST field during 2081–2100. Its average value in the simulation outer domain is +0.80 °C.

It is noted that the simulation start date was taken sufficiently early (about 10 days before the time of landfall) for the system to have the time to adjust to changes in the initial SSTs, and for all atmospheric fields to be fully physically and thermodynamically consistent by the time of landfall. More specifically, warmer initial SSTs resulted in an increase in evaporation at the beginning of the simulation, which ultimately modified the three-dimensional atmospheric fields, including the increase in atmospheric moisture. Fig. 5 shows the evolution of the PW averaged over the ocean grid points in the outer domain for the simulations that maximized the 72-h BA PD in the different SST increase scenarios. It is observed that, at the beginning of the simulation, all curves start from the same point with an average PW of about 43.6 mm. With time, the curves first diverge from each other for 4 to 5 days, after which the increase in PW due to the adjustment stabilizes. As expected, the larger the initial SST increase, the larger the average PW in the simulation domain. In this context, it may seem legitimate to think that the maximum PD over the target area will also increase as initial SSTs are increased.

4. Simulation results

Results for the PB-ST of Hurricane Ivan for each of the SST increase scenarios are given in Fig. 6. This figure shows the graphs of the 72-h BA PD for the different scenarios as a function of the shifting amount along the shifting transect. Interestingly, it is observed that the general structure of the graph changes substantially from one case to another, as opposed

---

[8] In Mure-Ravaud et al. (2019a), however, the TC vortex in the ICs for the simulation of Hurricane Ivan was shifted in a direction orthogonal to the TC track using 29 increments of shift only, from 1.67°W/7.18°S to 1.67°E/7.18°N.

[9] The Community Climate System Model version 4 (CCSM4) is a coupled climate model developed by NCAR to simulate the global climate system (Gent et al., 2011). The model is composed of five separate components which simulate the Earth's atmosphere, ocean, land, land-ice, and sea-ice simultaneously. It has a horizontal grid resolution of approximately 1.25° × 0.94° and 26 layers in the vertical direction.

[10] Representative Concentration Pathways (RCPs) are greenhouse gas concentration trajectories for the future (Moss et al., 2010; van Vuuren et al., 2011). They describe a total of four possible climate futures: one mitigation scenario (RCP 2.6), two intermediate stabilization scenarios (RCP 4.5 and RCP 6.0), and one very high baseline emission scenario (RCP 8.5). The numerical values of the RCP scenarios represent the radiative forcing values of the year 2100 relative to pre-industrial levels, measured in watts per square meter (W m^{-2}) (Clarke et al., 2007; van Vuuren et al., 2011).

Table 1
Parameterization schemes used for the simulation of Hurricane Ivan.

Parameterization	Name of the scheme
Microphysics	WRF double moment 6-class (WDM6)
Cumulus[a]	New Simplified Arakawa-Schubert (SAS)
Planetary boundary layer	Mellor-Yamada-Janjic (MYJ)
Longwave radiation	Rapid Radiative Transfer Model (RRTM)
Shortwave radiation	Dudhia
Land surface	Unified Noah land-surface model
Surface layer	Monin-Obukhov (Janjic Eta)

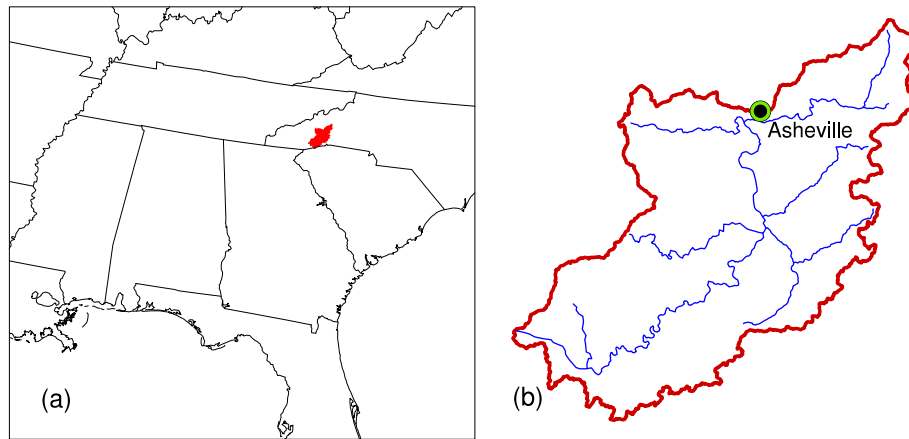[a] Cumulus parameterization was only used in the outer and intermediate domains.

Fig. 3. Target area used for the PB-ST. (a) The target area is shown in red within the simulation inner domain. (b) The target area corresponds to the drainage basin of the city of Asheville, NC.
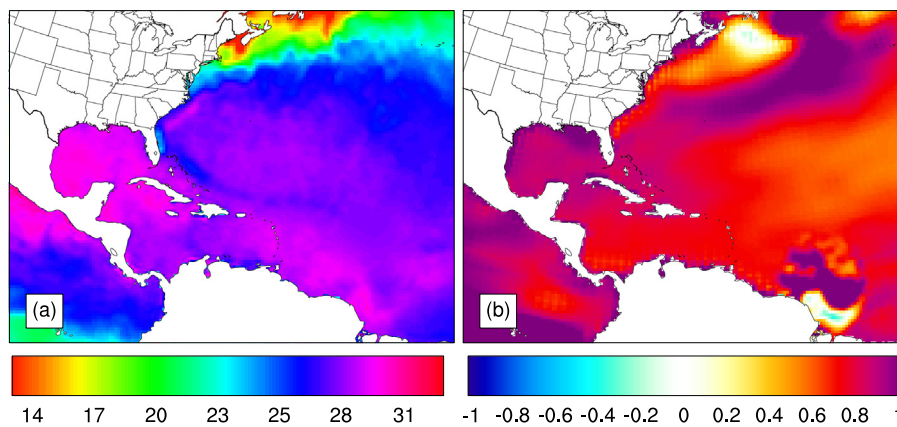

Fig. 4. (a) Sea surface temperature (SST; °C) field on 09/06/2014 00:00 UTC (simulation start date). (b) SST climate change (CC) perturbation field obtained by subtracting the mean SST field in CCSM4 RCP 4.5 for 2005–2024 from the mean SST field for 2081–2100.

to an expected simple translation of the PD graph in the direction of the change of SST. In particular, the maximum PDs (given by the red diamonds) do not even occur for the same shifting amount.

From Fig. 6, the average 72-h BA PD was obtained by calculating the areas under the curves and dividing these areas by the range of shifting amounts. Fig. 7 shows how the average 72-h BA PD and the maximum 72-h BA PD (given by the red diamonds in Fig. 6) change as the initial SST is modified. As expected, as the SST increases, the average PD also increases, from 93 mm for no increase in SST to 147 mm for a spatially

Fig. 5. Evolution of the PW (mm) averaged over the ocean grid points in the outer domain for the simulations which maximized the 72-h BA PD in the different SST increase scenarios (whose tracks are given in Fig. 9).

constant increase of 2 °C. Although the average value of the spatially varying SST perturbation field (Fig. 4b) is +0.80 °C, it is observed that the average 72-h BA PD is in this case about the same as for the case of a spatially constant SST increase of 1 °C, which shows that the spatial distribution of the SST does play a role in determining the behavior of a TC and the intensity of its PD field.

Moreover, Fig. 7b shows that the maximum 72-h BA PD has a different behavior than the average 72-h BA PD. Surprisingly, the largest 72-h BA PD was obtained in the case of no SST increase. However, if the second largest peak in Fig. 6a is considered instead of the largest peak (given by the red diamond), the maximum 72-h BA PD increases almost linearly with the spatially constant SST increment. As a result, it may be hypothesized that, in the case of no SST increase, the behavior of the TC in the simulation maximizing the 72-h BA PD is fundamentally different than in the SST increase scenarios. On the other hand, in these scenarios, it is likely that the TCs of the simulations that maximized the 72-h BA PD have a similar behavior, so that larger PDs, obtained for larger SSTs, are simply due to the increase in IVT convergence. In addition, the maximum PD obtained in the case of the spatially varying CC SST perturbation, for which the mean SST increase is +0.80 °C, is about as large as the maximum PD obtained in the case of a spatially constant SST increase of 2 °C. This shows, once again, that the spatial distribution of the SST in the ICs is important in determining the behavior of the system.

5. Discussion

First, the fact that the general structure of the graph of the 72-h BA PD as a function of the shifting amount in Fig. 6 substantially changes
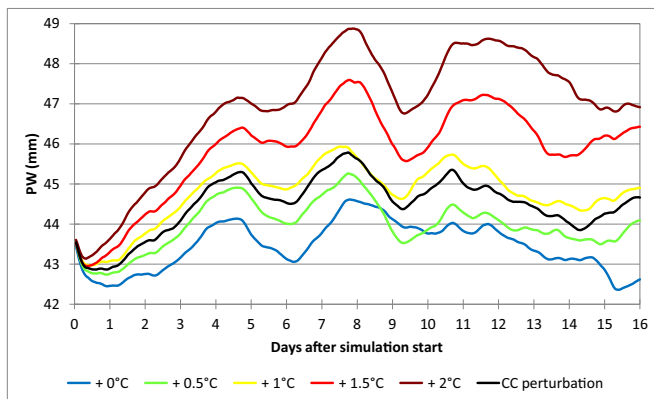
from one SST increase scenario to another shows that an increase in SST in the ICs, which ultimately translates into an increase in atmospheric moisture during the simulation, leads to significant changes in Hurricane Ivan's track. As a result, it is impossible to infer the TC behavior for the warmer conditions from the TC behavior for the original conditions.

These findings put into question the legitimacy of the traditional moisture maximization approach used for PMP estimation, as discussed in Section 1. Indeed, by maximizing IP from a storm by the ratio of the maximum to the actual PW, this approach implicitly assumes that the underlying wind velocity field responsible for moisture transport remains unchanged. If this were truly the case, given the almost one-to-one relationship between IVT convergence and PD (see Mure-Ravaud et al. (2019b) and Appendix A), and given the linearity of the divergence operator, multiplying the PW by a given ratio would indeed cause the PD to be also approximately multiplied by the same ratio. However, the numerical experiments performed in this study show that the wind field does not remain unchanged when the atmospheric moisture is enhanced, which should not be surprising since the momentum conservation equations, energy conservation equation, and water vapor conservation equation of the fully compressible Euler equations solved by WRF are coupled.

Fig. 8 presents the 1-week PD fields, IVT fields and IVT divergence fields for the simulations maximizing the 72-h BA PD. Not surprisingly, the regions of large IVT convergence overall closely match the regions of IP. In all cases except for the one with no increase in SST, these fields look alike in the region around the target area, although they generally look different more downstream from this region due to different locations of landfall. More precisely, around the target area, the PD fields are characterized by a southwest-northeast oriented band of very IP, which exactly coincides with the location and orientation of the Appalachian Mountains in this region. In the case of no SST increase (Fig. 8a and b), the structures of the PD field, IVT field, and IVT divergence field are different from the other cases. In this case, the PD field is significantly larger and more intense in the southern and central Appalachian region due to a much larger IVT convergence. The large IVT convergence seems to be due not only to a decrease in the IVT magnitude in the direction of the flow as for the other cases, but also to a change in direction of the IVT field in this region from northward to westward.

The different TC behaviors between the case of no SST increase and the other cases become evident when examining Fig. 9. This figure shows the TC tracks for the simulations maximizing the 72-h BA PD obtained by following the TC's center of low sea level pressure (SLP). The advantage of using the SLP field to evaluate the TC track is that the TC's center of low SLP remains well defined even after landfall, so that the TC track can also be followed inland. The TC track for the case of no SST increase is shown in blue, and it is observed to substantially differ from the other tracks. Indeed, the TC tracks corresponding to increased initial SSTs passed either over or slightly off western Cuba. On the other hand, the TC in the case of no SST increase went further south and passed over the Yucatán Peninsula, after which its track
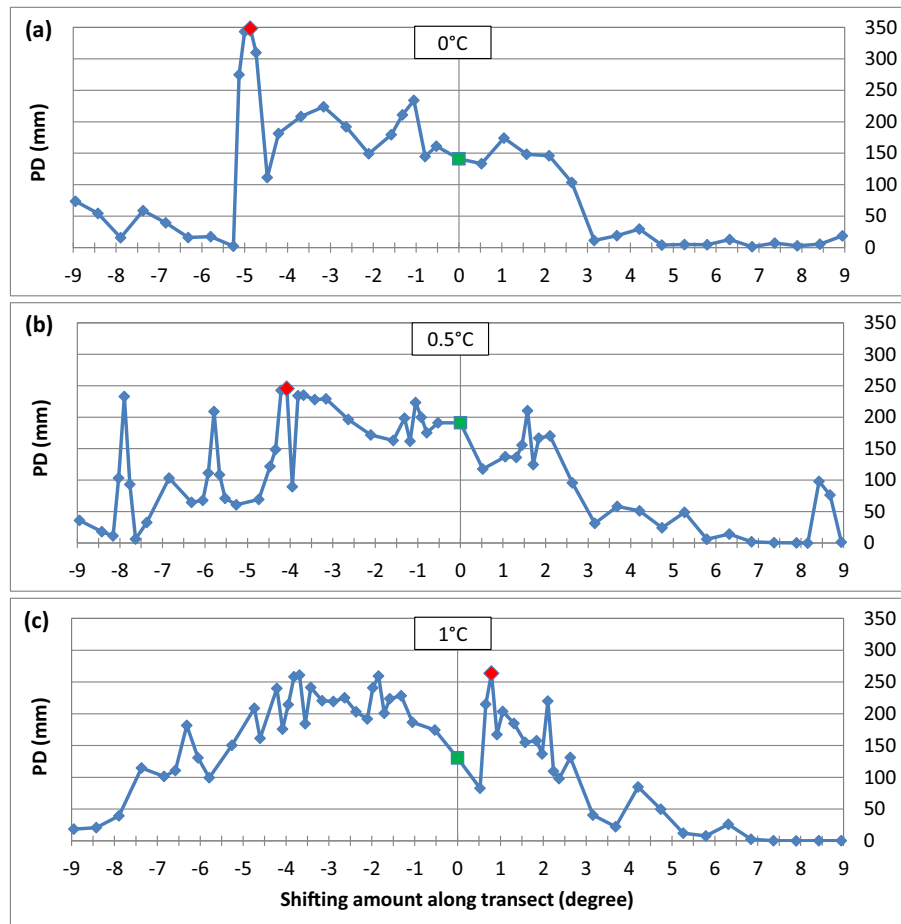
Fig. 6. 72-h BA PD as a function of the amount of shift along the shifting transect (corresponding to the black double-headed arrow in Fig. 1) for (a) no change in SST, (b) a spatially constant SST increase of 0.5 °C, (c) a spatially constant SST increase of 1 °C, (d) a spatially constant SST increase of 1.5 °C, (e) a spatially constant SST increase of 2 °C, and (f) the (spatially varying) CC perturbation field of Fig. 4b. Negative shifting amounts correspond to a shift to the left of the TC track, whereas positive values are for a shift to the right of the TC track. The green squares give the 72-h BA PD for zero shift. The red diamonds give the maximum 72-h BA PD.
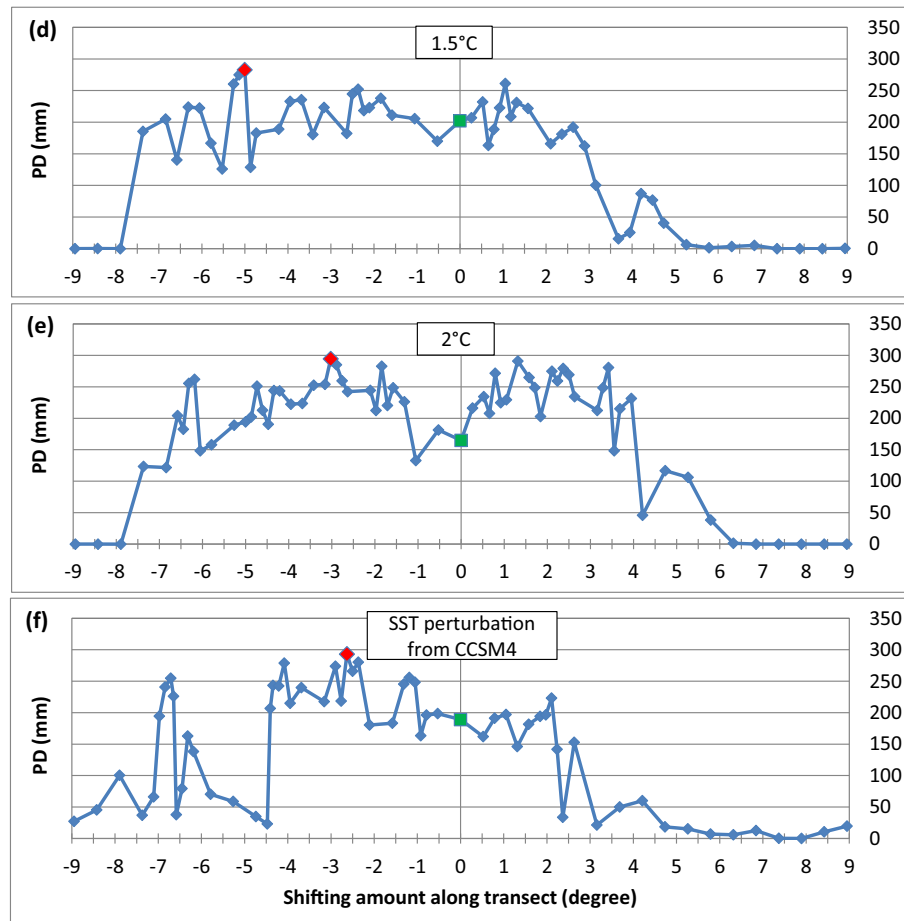
Fig. 6 (*continued*).

recurved northeastwards, unlike the other TC tracks which were mostly northwards.

Most importantly, while the TC tracks corresponding to the increased initial SSTs passed west of the Appalachian Mountains and continued northwards, the TC track for no SST increase had a more complicated behavior. In this case, the TC slid eastwards along the southern extremity of the Appalachian Mountains, which brought it into Southern Carolina where its track turned back southwards. This complex behavior made the TC stay in the simulation inner domain for a longer period than in the other cases, as highlighted in Table 2. Table 2 shows that the TC's center of low SLP stayed in the inner domain for 110 h in the case with no increase in the SST, which is 2 to 3 times longer than in the other cases. Hence, the different track, obtained in the case of no SST increase, and the longer time spent in the inner domain both explain why the 72-h BA PD was larger in this case as compared to the other cases involving increased SSTs.

6. Conclusions

In this article, numerical experiments consisting of increasing the SST in the ICs of the simulation of Hurricane Ivan (2004) were performed using the WRF model. This increase in the SST ultimately translated into an increase in the atmospheric water vapor during the simulation. A PB-ST method was then applied to each SST increase scenario, using the drainage basin of the city of Asheville, NC as a target area. Surprisingly, the maximum 72-h BA PDs for the different SST increase scenarios were not as large as in the case of no SST increase. Indeed, in this case, the TC had a significantly different track, especially
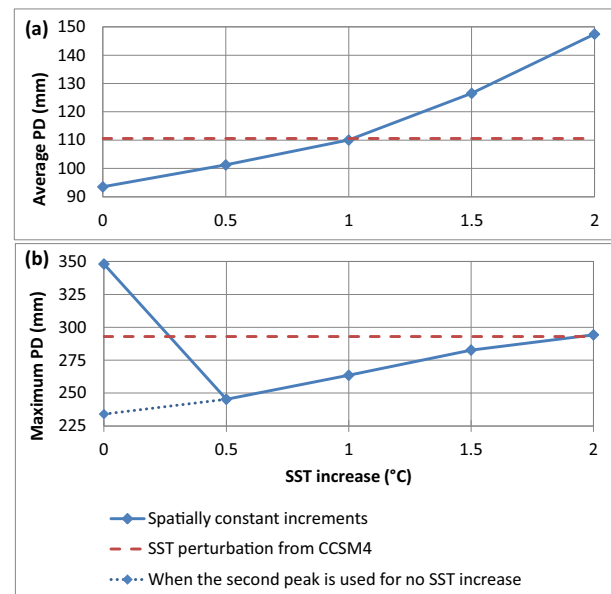

Fig. 7. (a) gives the average 72-h BA PD as a function of the SST increase at the simulation start date. These average PDs were computed by calculating the areas under the curves of Fig. 6 and by dividing these areas by the range of shifting amounts (about 18°). (b) gives the maximum 72-h BA PD (given by the red diamonds in Fig. 6) as a function of the SST increase. In both cases, the dashed red line shows the 72-h BA PD corresponding to the numerical experiments with the spatially varying CC SST perturbation field of Fig. 4b. The dotted blue line in (b) shows what the curve would look like if the second maximum of the 72-h BA PD for no SST increase (Fig. 6a) was taken instead of the maximum.

after landfall, and spent much longer in the simulation inner domain, thus resulting in a larger PD over the target area.

These results have implications regarding the assumptions made in some of the traditional PMP approaches using *moisture maximization* such as the generalized method. First, since the momentum conservation equations, energy conservation equation, and water vapor conservation equation of the fully compressible Euler equations solved by WRF are coupled, and given the strong nonlinearity involved in the dynamics and thermodynamics of TCs, increasing the atmospheric moisture will most likely cause significant changes in the track of a TC, so that this increase may actually lead to a decrease of the PD over the target area. Secondly, in the case of TCs, the magnitude of the atmospheric moisture is just one element among many others responsible for the intensity of the PD field. In fact, it was found that the spatiotemporal behavior of the IVT field including its interaction with local features such as topography is a much more important factor in the generation of IP because this behavior eventually conditions where and to what extent moisture will converge over a given region, thus causing IP in this region. These findings also show that if Hurricane Ivan happens again in the future, under warmer and moister conditions, PDs produced by the storm may not necessarily exceed those produced in 2004.
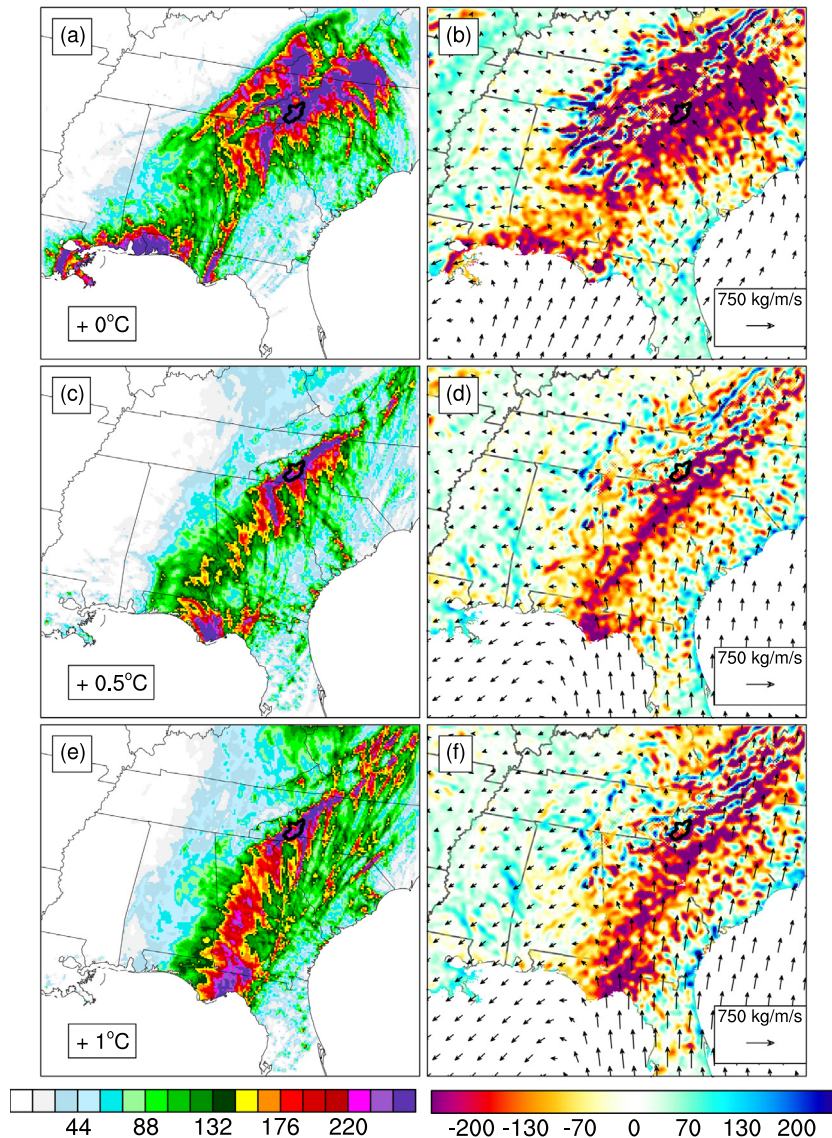
Acknowledgments

Fig. 8. The left column shows the 1-week PD (mm) fields of the simulations maximizing the 72-h BA PD for the different scenarios of SST changes. These 1-week periods are such that their last 72 h are the time period for which the maximum 72-h BA PD was attained, which corresponds to the following end dates: (a) (b) 09/19/2004 08:00 UTC, (c) (d) 09/16/2004 00:00 UTC, (e) (f) 09/15/2004 12:00 UTC, (g) (h) 09/16/2004 04:00 UTC, (i) (j) 09/15/2004 22:00 UTC, and (k) (l) 09/15/2004 23:00 UTC. The right column presents the associated 1-week-average IVT (kg m^{-1} s^{-1}) fields and IVT divergence (mm) fields. The target area is the polygon bounded by a bold black line in the western Carolinas.
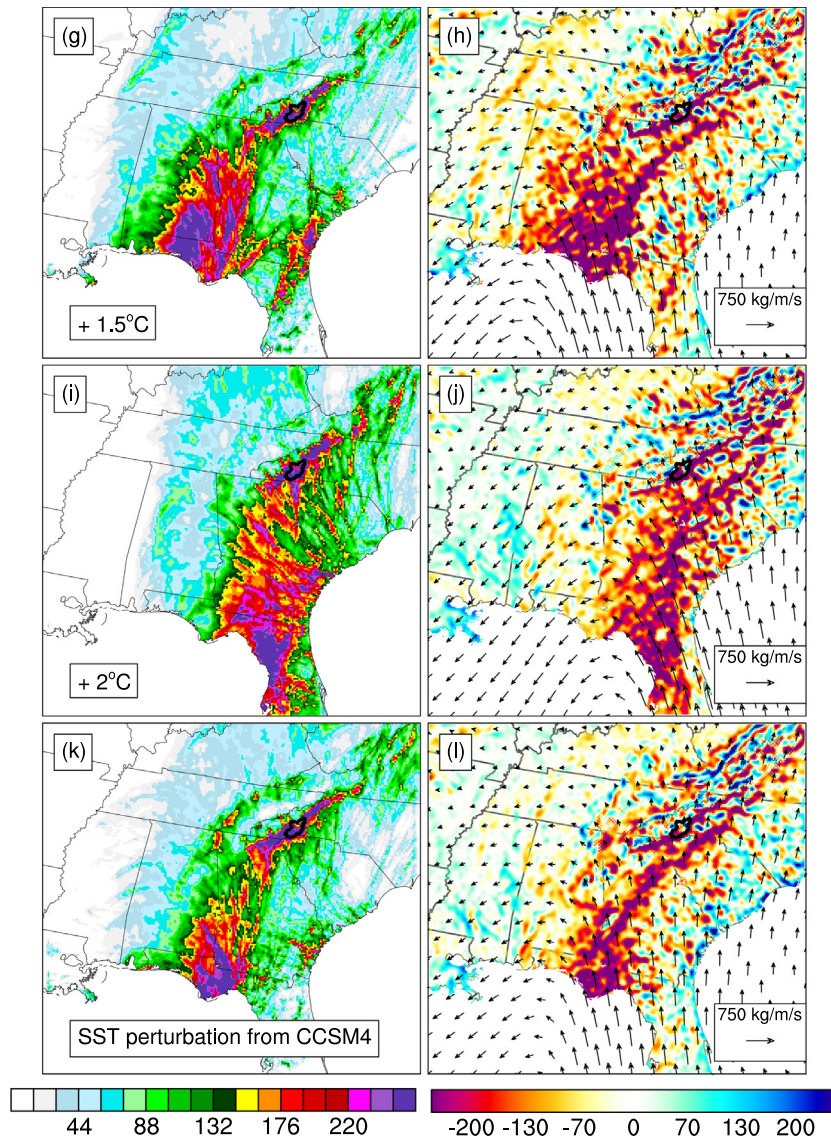
Fig. 8 (*continued*).

Appendix A

The set of model physics options (i.e. parameterization schemes) used for the simulation of Hurricane Ivan and reported in Table 1 are those used in Mure-Ravaud (2019). This study is a Ph.D. thesis (to be submitted to the Office of Graduate Studies of the University of California, Davis in May 2019) entitled *On the Maximization of Precipitation from Tropical Cyclones in the Context of Climate Change*. In the first chapter, the PD fields and moisture transport fields of 13 TCs during 1999–2016, including Hurricane Ivan, were reconstructed with the WRF model.

Due to the strong nonlinearity involved in a TC's dynamics and thermodynamics, placing a TC's PD field in the observed location can be challenging. In Mure-Ravaud (2019), this was achieved by trying several simulation start dates and combinations of the WRF model's parameterization schemes for each event. The parameterization schemes combination given in Table 1 is the combination which provided the most satisfactory results for the reconstruction of Hurricane Ivan's PD field in terms of its location, structure, and intensity.

More specifically, in Mure-Ravaud (2019), the performance of the WRF model in reconstructing the PD field of a TC was evaluated in two steps. First, the simulated and observed PD fields were plotted and visually compared. Although subjective, such visual examination is a rapid and powerful way to eliminate unrealistic simulations because the human brain is able to analyze at once many aspects of the results such as the general two-dimensional spatial distribution of the PD field, which may be difficult to assess using goodness-of-fit statistics. Secondly, the model performance for the simulations offering satisfactory visual results was further assessed by using three metrics. These metrics were 1) the relative error in the inner-domain-averaged total PD which assesses whether the model adequately simulated the total precipitation amount in the simulation inner domain over the period of interest, 2) the overlap percentage for several PD thresholds which assesses whether the model placed the PD field in the observed location, and 3) the PD field area ratio (PDFAR) which compares the relative sizes of the observed and simulated PD fields above several PD thresholds.

In this appendix, for the sake of brevity, only the plot of the PD field and moisture transport fields in Hurricane Ivan are presented. Results in terms of the metrics and additional information may be found in Mure-Ravaud (2019) and in Mure-Ravaud et al. (2019b). Thus, the observed and simulated PD fields as well as the IVT field and IVT divergence field for Hurricane Ivan are provided in Fig. 10.
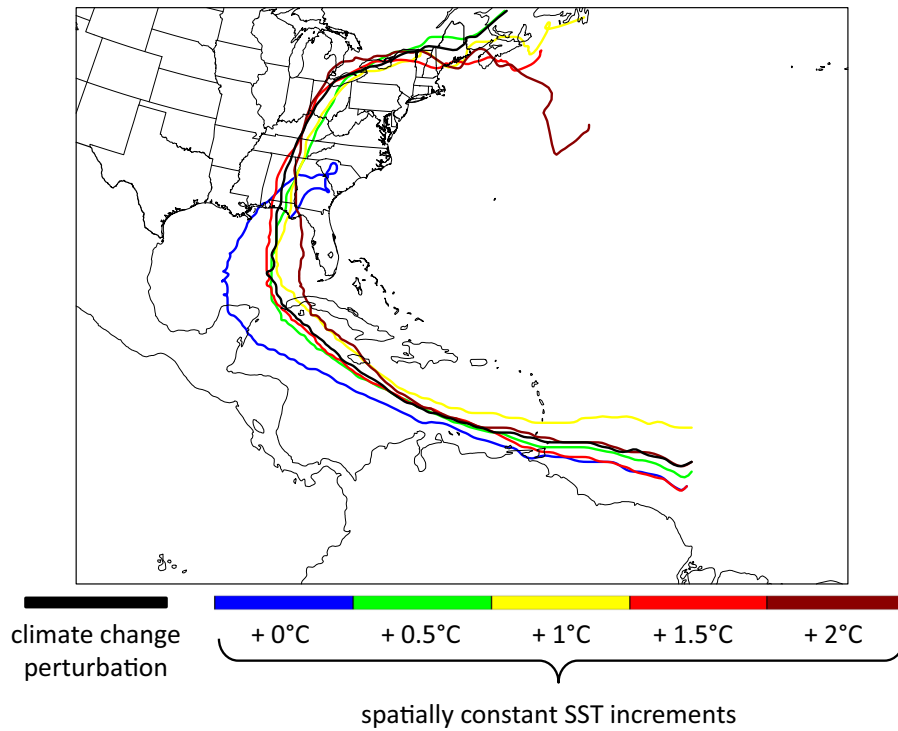
climate change
perturbation

+ 0°C + 0.5°C + 1°C + 1.5°C + 2°C

spatially constant SST increments

Fig. 9. TC tracks for the simulations maximizing the 72-h BA PD and for the different SST increase scenarios.

Table 2
Time spent by the TC's center of low sea-level pressure (SLP) in the simulation inner domain.

	Spatially constant SST increments					Climate change perturbation
	0 °C	0.5 °C	1 °C	1.5 °C	2 °C	
Time spent in inner domain (h)	110	43	39	37	37	40

Fig. 10 shows that the WRF model performed well in simulating the location, structure, and intensity of Hurricane Ivan's PD field. Besides, a strong connection is observed between PD on the one hand and IVT divergence on the other hand. In particular, the regions of intense PD overall clearly match the regions of intense IVT convergence. Fig. 11 quantitatively illustrates this relationship. It provides the graph of
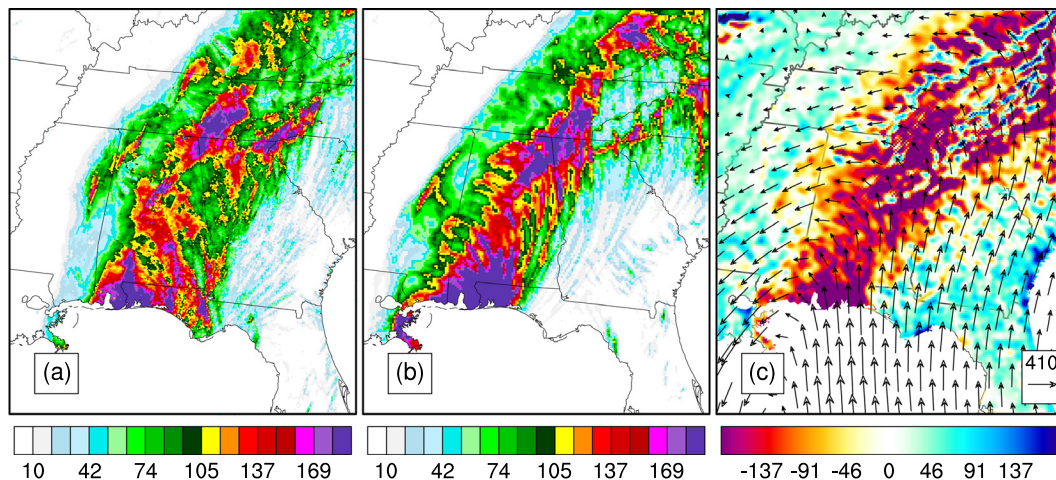

Fig. 10. Inner domain observations and simulation results for Hurricane Ivan for the time period 09/14/2004 00:00 to 09/19/2004 00:00. (a) Observed PD (mm); (b) simulated PD (mm); (c) vectors: time averaged IVT (kg m^{-1} s^{-1}). Color map: divergence of the time-averaged IVT field (mm).
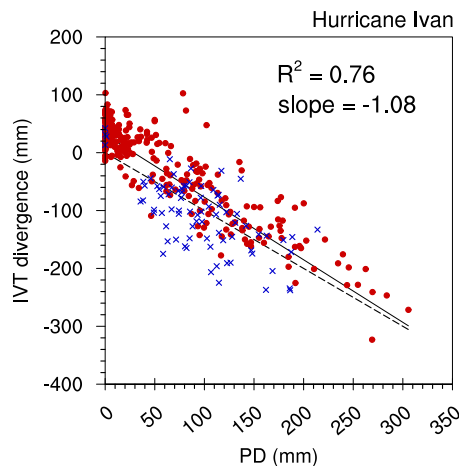From Mure-Ravaud (2019).

Fig. 11. Divergence of the time-averaged IVT field (mm) as a function of the PD (mm) for Hurricane Ivan. Red dots correspond to the locations where the ground surface elevation is below the 80th percentile of the ground surface elevation in the inner domain. Blue crosses correspond to the locations where the ground surface elevation is above this threshold. The solid black line is the regression line. Its associated coefficient of determination (R^2) and slope are given on the figure. The dashed line is the bisector line; it has a slope of −1 and an intercept of 0.
From Mure-Ravaud (2019).

the divergence of the time-averaged IVT field as a function of the PD. It is noted that, since the inner domain contains a large number (199×232) of grid points, the IVT divergence field and the PD field were averaged towards a coarser grid containing 400 grid points (corresponding to a 20×20 grid in the case of a square inner domain) in order to facilitate the analysis of the dependence of the PD on IVT divergence. In Fig. 11, a linear regression was also performed, and the coefficient of determination (R^2) as well as the slope of the regression line (solid black line) are provided. The bisector line, defined as the line with a slope of −1 and an intercept of 0 is also shown as a dashed black line. Eventually, grid points in the most elevated portion of the inner domain, defined as the region above the 80th percentile of the ground surface elevation, are given by blue crosses whereas other grid points are represented by red dots.

It is observed that the coefficient of determination is relatively large ($R^2 = 0.76$) and that the slope of the regression line is close to −1. This shows the strong correlation between PD and IVT divergence. In addition, in Fig. 11, most of the blue crosses representing grid points in the most elevated regions of the inner domain lie below the regression line, and even below the bisector line (which strongly participates in reducing the coefficient of determination). This shows that, at these elevated grid points, the PD was not as intense as the associated IVT convergence.

References

Casas, M.C., Rodríguez, R., Nieto, R., Redaño, A., 2008. The Estimation of Probable Maximum Precipitation. Ann. N. Y. Acad. Sci. 1146, 291–302. https://doi.org/10.1196/annals.1446.003.

Casas, M.C., Rodríguez, R., Prohom, M., Gázquez, A., Redaño, A., 2011. Estimation of the probable maximum precipitation in Barcelona (Spain). Int. J. Climatol. 31, 1322–1327. https://doi.org/10.1002/joc.2149.

Clarke, L., Edmonds, J., Jacoby, H., Pitcher, H., Reilly, J., Richels, R., 2007. Scenarios of Greenhouse Gas Emissions and Atmospheric Concentrations.

Corrigan, P., 1999. Probable Maximum Precipitation for California. National Weather Service.

Gent, P.R., Danabasoglu, G., Donner, L.J., Holland, M.M., Hunke, E.C., Jayne, S.R., Lawrence, D.M., Neale, R.B., Rasch, P.J., Vertenstein, M., Worley, P.H., Yang, Z.-L., Zhang, M., 2011. The community climate system model version 4. J. Clim. 24, 4973–4991. https://doi.org/10.1175/2011JCLI4083.1.

Hershfield, D.M., 1961. Estimating the probable maximum precipitation. J. Hydraul. Div. 87, 99–116.

Hershfield, D.M., 1965. Method for Estimating Probable Maximum Rainfall. J. Am. Water Works Assoc. 57, 965–972. https://doi.org/10.1002/j.1551-8833.1965.tb01486.x.

Hurricane Research Division - Atlantic Oceanographic & Meteorological Laboratory, d. Frequently asked questions: what is a "Cape Verde" hurricane? http://www.aoml.noaa.gov/hrd/tcfaq/A2.html, Accessed date: 22 February 2019

Kulkarni, B.D., Nandargi, S., Mulye, S.S., 2010. Zonal estimation of probable maximum precipitation rain depths over the Krishna basin in peninsular India. Hydrol. Sci. J. 55, 93–103. https://doi.org/10.1080/02626660903529015.

Meteorology Glossary of the American Meteorological Society, 2015. Precipitable water. http://glossary.ametsoc.org/wiki/Precipitable_water (last accessed on 02/22/2019).

Moss, R.H., Edmonds, J.A., Hibbard, K.A., Manning, M.R., Rose, S.K., Van Vuuren, D.P., Carter, T.R., Emori, S., Kainuma, M., Kram, T., others, 2010. The next generation of scenarios for climate change research and assessment. Nature 463, 747.

Mure-Ravaud, M., 2019. On the Maximization of Precipitation From Tropical Cyclones in the Context of Climate Change. University of California, Davis.

Mure-Ravaud, M., Dib, A., Kavvas, M.L., Yegorova, E., Kanney, J., 2019a. Physically based storm transposition of four Atlantic tropical cyclones. Sci. Total Environ. https://doi.org/10.1016/j.scitotenv.2019.02.141.

Mure-Ravaud, M., Ishida, K., Kavvas, M.L., Yegorova, E., Kanney, J., 2019b. Numerical reconstruction of the intense precipitation and moisture transport fields for six tropical cyclones affecting the eastern United States. Sci. Total Environ. https://doi.org/10.1016/j.scitotenv.2019.02.185.

National Geographic Society, 2011. Precipitation. https://www.nationalgeographic.org/encyclopedia/precipitation/ (last accessed on 02/22/2019).

National Weather Service, d. Dew Point vs Humidity. https://www.weather.gov/arx/why_dewpoint_vs_humidity, Accessed date: 22 February 2019.

Rakhecha, P.R., Soman, M.K., 1994. Estimation of probable maximum precipitation for a 2-day duration: part 2 − north Indian region. Theor. Appl. Climatol. 49, 77–84. https://doi.org/10.1007/BF00868192.

Saha, S., Moorthi, S., Pan, H.-L., Wu, X., Wang, J., Nadiga, S., Tripp, P., Kistler, R., Woollen, J., Behringer, D., Liu, H., Stokes, D., Grumbine, R., Gayno, G., Wang, J., Hou, Y.-T., Chuang, H.-Y., Juang, H.-M.H., Sela, J., Iredell, M., Treadon, R., Kleist, D., Van Delst, P., Keyser, D., Derber, J., Ek, M., Meng, J., Wei, H., Yang, R., Lord, S., van den Dool, H., Kumar, A., Wang, W., Long, C., Chelliah, M., Xue, Y., Huang, B., Schemm, J.-K., Ebisuzaki, W., Lin, R., Xie, P., Chen, M., Zhou, S., Higgins, W., Zou, C.-Z., Liu, Q., Chen, Y., Han, Y., Cucurull, L., Reynolds, R.W., Rutledge, G., Goldberg, M., 2010a. NCEP Climate Forecast System Reanalysis (CFSR) 6-Hourly Products, January 1979 to December 2010.

Saha, S., Moorthi, S., Pan, H.-L., Wu, X., Wang, J., Nadiga, S., Tripp, P., Kistler, R., Woollen, J., Behringer, D., et al., 2010b. The NCEP climate forecast system reanalysis. Bull. Am. Meteorol. Soc. 91, 1015–1057. https://doi.org/10.1175/2010BAMS3001.1.

Saha, S., Moorthi, S., Wu, X., Wang, J., Nadiga, S., Tripp, P., Behringer, D., Hou, Y.-T., Chuang, H., Iredell, M., Ek, M., Meng, J., Yang, R., Mendez, M.P., van den Dool, H., Zhang, Q., Wang, W., Chen, M., Becker, E., 2011. NCEP Climate Forecast System Version 2 (CFSv2) 6-Hourly Products.

Saha, S., Moorthi, S., Wu, X., Wang, J., Nadiga, S., Tripp, P., Behringer, D., Hou, Y.-T., Chuang, H., Iredell, M., Ek, M., Meng, J., Yang, R., Mendez, M.P., van den Dool, H., Zhang, Q., Wang, W., Chen, M., Becker, E., 2014. The NCEP Climate Forecast System Version 2. J. Clim. 27, 2185–2208. https://doi.org/10.1175/JCLI-D-12-00823.1.

Skamarock, W.C., Klemp, J.B., 2008. A time-split nonhydrostatic atmospheric model for weather research and forecasting applications. J. Comput. Phys. 227, 3465–3485. https://doi.org/10.1016/j.jcp.2007.01.037.

Stewart, S.R., 2004. Tropical Cyclone Report Hurricane Ivan 2–24 September 2004. Natl. Hurric. Cent.

Tingsanchali, T., Tanmanee, S., 2012. Assessment of hydrological safety of Mae Sruai Dam, Thailand. Procedia Eng. 32, 1198–1204.

van Vuuren, D.P., Edmonds, J., Kainuma, M., Riahi, K., Thomson, A., Hibbard, K., Hurtt, G.C., Kram, T., Krey, V., Lamarque, J.-F., Masui, T., Meinshausen, M., Nakicenovic, N., Smith, S.J., Rose, S.K., 2011. The representative concentration pathways: an overview. Clim. Chang. 109, 5. https://doi.org/10.1007/s10584-011-0148-z.

World Meteorological Organization, 2009. Manual on Estimation of Probable Maximum Precipitation (PMP).

Zhan, D., Zhou, J., 1984. Recent developments on the probable maximum precipitation (PMP) estimation in China. J. Hydrol. 68, 285–293. https://doi.org/10.1016/0022-1694(84)90216-6.